[1]Numerical Study on C-axis Orientations of Sea Ice Surface Grown under Calm Sea Conditions using a Particle Method and Voronoi Dynamics

Yoshiki Kawano[2] and Tetsuya Ohashi[3]

[2]Department of Mechanical Systems Engineering, National Institute of Technology, Asahikawa College;
2-2 Shunkodai; Asahikawa, Hokkaido 0718142, Japan

[3]Department of Mechanical Engineering, Kitami Institute of Technology;
165 Koencho; Kitami, Hokkaido 0908507, Japan

E-mail: [2]kawano@asahikawa-nct.ac.jp; [3]ohashi@newton.mech.kitami-it.ac.jp

[1]The paper is based on a preliminary study published by Kawano and Ohashi (2013).

Abstract

Physical properties of frazil and grease ice depending on their microstructures are not easily measured, while they are important elements for predicting their behavior on the ocean surface. Thus, numerical models considering the effect of the microstructures are required to investigate the ice-water mixture. In this paper, we combined a computational fluid dynamics (CFD) and crystal growth model, and numerically predicted a process of flotation and accumulation of crystal nuclei near the surface of calm sea, and their growth after the accumulation. The results obtained showed that the crystal fabrics and c-axis distributions had good similarity with those of an actual sea ice, and the combined model was effective for dealing with ice-water mixture. Thus far, while we have paid little attention to the details of c-axis distributions within the surface layer of sea ice because of their tedious investigation, the results also indicated that anisotropic growth of crystal nuclei, as well as the flotation and accumulation, strongly affects the c-axis distributions within the horizontal cross-sections of the surface layer of sea ice grown under calm sea conditions. This work would be an important step for the development of numerical models to predict the complex phenomena of sea ice depending on the microstructures, such as behavior of the ice-water mixture on the sea surface.

Keywords: Sea ice; Crystal growth; Numerical simulation; C-axis orientations; Flotation of crystal nuclei; Geometric selection

1. Introduction

Sea ice is mainly comprised of pure ice crystals arranged in an hcp lattice and brine inclusions. They influence mechanical (e.g., Zhan and Wilson, 1997; Schulson, 1999; Cole, 2001), thermal, and other properties (e.g., Gow and Tucker III, 1991) of sea ice, thus requiring detailed studies. However, the characteristics of sea ice can be considerably altered by changes in the growth conditions and the environment in which it exits (e.g. Weeks and Ackley, 1986; Weeks, W.F., 1998; Golden et al., 1998; Eicken, 2003; Jones et al., 2013); this fact makes it difficult to perform experimental studies under laboratory conditions.

In many cases, sea ice growth initiates from the ice crystal nuclei generated in supercooled seawater (e.g, Weeks and Ackley, 1986; Eicken, 2003). Nuclei grow into spherical and then discoidal crystals before forming a dendritic shape, and float to and accumulate near the sea surface (e.g. Weeks and Ackley, 1986). In leads and polynyas, generation of frazil ice is an important formation mechanism of sea ice (e.g. Martin, 1981; Ushio and Wakatsuchi, 1993; Smedsrud et al., 2006; Skogseth et al, 2009), and solid fraction of the grease ice formed by their accumulation is matter of deep interest (e.g. Naumann et al, 2012; Maus and De La Rosa, 2012); however, it is fiendishly difficult to measure. Thus, numerical models to investigate the solid fraction would be useful and powerful tools in the studies of ice-water mixture.

A number of numerical models have been developed. For example, Petrich et al. (2006) used a computational fluid dynamics model to simulate the unidirectional growth of sea ice and successfully obtained c-shape profiles of salinity, which are typically observed in first-year sea ice (e.g., Gow and Tucker III, 1991; Eicken, 2003). Maus and De la Rosa (2012) developed mathematical model to predict salinity and solid fraction of frazil and grease ice, and successfully reproduced them. In their model, however, seawater solidification processes were predicted using a continuum approximation and the orientation of each crystal was not considered. The amount of seawater in the grease ice would be influenced by changes of the geometry of ice nuclei accumulated near the sea surface. Thus, growth rate anisotropies of the nuclei have to be considered to predict the amount of seawater trapped in the ice; that is, we require the consideration of crystal orientations in the numerical models.

The crystal fabric of typical first-year sea ice is known to show fine grains in the uppermost surface and columnar-shaped grains below it. This transition in the shape and size of grains accompanies a change in c-axis orientations. In other words, the c-axes of crystals show various directions within the layer of fine crystals and gradually align in the horizontal direction within the layer below with depth. The mechanisms of the transition process of c-axis orientations to the horizontal direction are known as geometric selection (e.g., Weeks and Ackley, 1986; Weeks and Wettlaufer, 1996); however, little attention has been paid to the c-axis orientations within the layer of fine grains near the sea surface. A reason for this is that the diameter of grains in this layer is usually <5 mm and such fine

88 grains are tedious to investigate using traditional experimental methods in glaciology
89 (Weeks and Wettlaufer, 1996).
90
91 Kawano and Ohashi (2009) have conducted numerical simulations of the development of
92 the crystal fabric of sea ice using the Voronoi dynamics technique (Ohashi et al., 2004).
93 In the model, the development of the crystal fabric was represented by the growth of crystal
94 nuclei that had an anisotropic growth rate, and alignment of c-axes within the horizontal
95 plane by geometric selection was obtained. In the simulation, however, the positions of
96 crystal nuclei were fixed and their orientations, that were randomly selected, also remained
97 at their initial states, and the flotation and rotation of crystal nuclei during their growth
98 were not considered.
99
100 Recently, Dempsey et al. (2010) introduced the effect of rotation of crystals into the
101 Voronoi dynamics technique, and successfully reproduced the development process of the
102 crystal fabric of platelet ice. In their model, the process of flotation of platelets was
103 ignored, and only the rotation after flotation was considered; each platelet rested at the
104 orientation where three or more points on the surface were in contact with the bottom of the
105 sea ice. Thus, the orientations were decided only by the mechanical stability, and the
106 effects of fluid dynamics and buoyancy on platelets were not directly considered (Dempsey
107 et al., 2010).
108

In this study, we first employed a computational fluid dynamics (CFD) model to represent a process of growth and accumulation of crystal nuclei with their flotation driven by the buoyancy, and simulated the formation process of the layer of fine crystals under calm sea conditions. However, the CFD simulation is computationally expensive; we conducted it by a two-dimensional approximation. We second investigated each c-axis orientation of crystal nuclei in the accumulated layer near the sea surface, which was predicted by the above flotation and accumulation simulation, and we adapted the c-axis orientations to the initial crystal nuclei; a development process of sea ice crystal from the crystal nuclei was represented in the three-dimensional simulation space, using the Voronoi dynamics technique. Finally, we obtained numerical results for the development process of sea ice crystals from the sea surface and compared the c-axis distributions obtained with simulations and experiments (Weeks and Ackley, 1986), and validated the numerical models and investigated c-axis distributions near the sea surface.

2. Numerical Procedure

2.1 Nucleus Flotation Model

We employed the Moving Particle Semi-implicit (MPS) method to represent flotation of crystal nuclei growing in the seawater. The MPS method was developed by Koshizuka

131 and Oka (1995) and as a particle method for the incompressible fluid analysis. In the
132 MPS method, continuums are represented by moving particles which are calculation points,
133 i.e., the view point is Lagrangian. The MPS method has advantages compared to
134 traditional finite element (FEM) methods or finite difference methods (FDM);
135 computational grids are not necessary, interfaces can be easily tracked, and large
136 deformations of continuums are easily represented. Thus, it has been applied to
137 simulations of complex phenomena such as breaking waves (e.g. Koshizuka et al., 1998;
138 Gotoh and Sakai, 2006), vapor explosions (e.g. Koshizuka et al., 1999), and fluid-structure
139 interactions (e.g., Koshizuka and Oka, 1995; Lee et al., 2007), as well as the incompressible
140 fluid simulations. The MPS method would also be a suitable for the simulations of
141 flotation of crystal nuclei growing in the seawater; that is because the method can easily
142 track the moving interfaces of ice-water and water-atmosphere, and represent the
143 interaction between crystal nuclei and seawater. The procedure was explained below.
144
145
146 **2.1.1 MPS Method for Incompressible Fluid**
147
148 To represent flotation of crystal nuclei in the seawater, the Navier-Stokes equation, given as
149 follows:
150

$$\frac{D\vec{u}}{Dt} = -\frac{1}{\rho}\nabla P + \nu\nabla^2\vec{u} + \vec{g} \qquad (1)$$

151

was solved with the incompressibility condition by using the MPS method (Koshizuka and Oka, 1996; Koshizuka et al., 1998; Gotoh and Sakai, 2006), where $\vec{u}$ is the velocity vector, ρ is the density of the element at a position, P is the pressure, ν is the kinematic viscosity, and $\vec{g}$ is the acceleration due to gravity. Eq. (1) is written for an element at a position. In the simulation, the continuum was discretized by three types of particles: water, ice, and wall, and each particle has a density ρ in accordance with the individual particle type. That is, the element and ρ are changed with changing the position. The flow of sea water can be represented by solving Eq. (1) with the MPS method, while a solid-liquid interaction model is also necessary to represent the flotation of crystal nuclei. The procedure for solving Eq. (1) with the MPS method was explained in this section, and the solid-liquid interaction model was described in the section 2.1.3.

In the MPS method, Gradient and Laplacian operators in Eq. (1) are discretized by following particle interaction models (Koshizuka and Oka, 1996; Koshizuka et al., 1998; Gotoh and Sakai, 2006):

$$\left\langle \nabla \phi \right\rangle_i = \frac{d}{n^0} \sum_{j \neq i} \left[\frac{\phi_j - \phi_i}{\left| \vec{r}_j - \vec{r}_i \right|^2} \left(\vec{r}_j - \vec{r}_i \right) w\left(\left| \vec{r}_j - \vec{r}_i \right| \right) \right], \tag{2}$$

$$\left\langle \nabla^2 \phi \right\rangle_i = \frac{d}{\lambda n^0} \sum_{j \neq i} \left[\left(\phi_j - \phi_i \right) w\left(\left| \vec{r}_j - \vec{r}_i \right| \right) \right], \tag{3}$$

$$\lambda = \frac{\sum_{j \neq i} \left| \vec{r}_j - \vec{r}_i \right|^2 w\left(\left| \vec{r}_j - \vec{r}_i \right| \right)}{\sum_{j \neq i} w\left(\left| \vec{r}_j - \vec{r}_i \right| \right)}, \tag{4}$$

where d is the number of space dimensions, ϕ is an arbitrary scalar, $\vec{r}$ is the position vector of a particle, w is the weight function, λ is the parameter that ensures that increases in variance are equal to the analytical solutions, n^0 is the constant value of the particle number density fixed for incompressibility, i is the number of a particle, and j is the number of a neighbor of the particle i. The particle number density for particle i is defined as follows:

$$n_i = \sum_{j \neq i} w\left(\left| \vec{r}_j - \vec{r}_i \right| \right). \tag{5}$$

The weight function employed in this study is defined as follows (Shao and Lo, 2003):

$$w\left(\left| \vec{r}_j - \vec{r}_i \right| \right) = \begin{cases} \dfrac{40}{7\pi r_e^{\,2}} \left(1 - 6 \left(\dfrac{\left| \vec{r}_j - \vec{r}_i \right|}{r_e} \right)^2 + 6 \left(\dfrac{\left| \vec{r}_j - \vec{r}_i \right|}{r_e} \right)^3 \right) & 0 \le \left| \vec{r}_j - \vec{r}_i \right| < 0.5 r_e \\ \dfrac{10}{7\pi r_e^{\,2}} \left(2 - 2 \left(\dfrac{\left| \vec{r}_j - \vec{r}_i \right|}{r_e} \right) \right) & 0.5 r_e \le \left| \vec{r}_j - \vec{r}_i \right| < r_e \\ 0 & r_e \le \left| \vec{r}_j - \vec{r}_i \right| \end{cases}, \tag{6}$$

where r_e is the finite distance of interaction between particles. Ataie-Ashtiani and Farhadi (2006) conducted dam-break simulations using the MPS method, and compared the

184 stability of the calculations between six types of weight functions. Their results showed
185 that Eq. (6) was the most stable among them.
186
187 Eq. (1) was solved with Eqs. (2)-(4) by the following steps:
188 (i) The initial conditions of n^0, particle velocities $\vec{u}_i^0$ and pressure P_i^0 were set.
189 (ii) The temporary particle velocities $\vec{u}_i^*$ and positions $\vec{r}_i^*$ were calculated:
190

$$\vec{u}_i^* = \vec{u}_i^N + \Delta t\left[\nu\nabla^2\left\langle\vec{u}\right\rangle_i^N + \vec{g}\right], \tag{7}$$

191

$$\vec{r}_i^* = \vec{r}_i^N + \Delta t u_i^*, \tag{8}$$

192
193 where N is the time step and Δt is the time increment of the current step.
194 (iii) The temporary particle number density n_i^* was calculated by Eq. (5).
195 (iv) The pressure Poisson equation was solved:
196

$$\left\langle\nabla^2 P\right\rangle_i^{N+1} = S, \tag{9}$$

197
198 where S is the source term of the equation. In this study, we employed the model in
199 Kondo and Koshizuka (2007) as the source term to suppress pressure oscillation during
200 the simulation.
201 (v) The pressure gradient term of Eq. (1) was calculated and the velocities and positions of

the particles were modified:

$$\vec{u}_i^{N+1} = \vec{u}_i^{*} - \frac{\Delta t}{\rho}\left\langle \nabla P \right\rangle_i^{N+1}, \tag{10}$$

$$\vec{r}_i^{N+1} = \vec{r}_i^{N} + \Delta t \vec{u}_i^{N+1}. \tag{11}$$

Incompressible fluid flow was represented by repeating steps (ii)-(v).

2.1.2 Boundary Condition for Free Surfaces

Let us assume a continuum such as a water column. When the continuum is discretized by particles, no particle exits in the region outside of the continuum. Thus, particle number densities (Eq. (5)) are lower at the particles on the free surface than those inside of the continuum, and we can find particles on the free surface by using the difference between the particle number densities. A particle that satisfies

$$n_i^{*} < \beta n^0 \tag{12}$$

is considered to be on the free surface (Koshizuka and Oka, 1996), where β is a parameter. In this study, the interface between seawater and atmosphere was treated as the free surface,

220 and $\beta = 0.97$ (Koshizuka and Oka, 1996; Koshizuka et al., 1998) was employed and
221 $P = 0$ was applied to particles on the free surface.
222
223
224 **2.1.3 Interaction between Ice Crystals and Fluid**
225
226 Ice crystals were treated as rigid bodies in this study. Interactions between the rigid
227 bodies and fluid are represented by particles with a fixed relative configuration (Koshizuka
228 et al., 1998). The algorithm to represent the interaction consists of following two steps.
229 First, the algorithm for the incompressible fluid explained in the section 2.1.1 is adapted to
230 the ice particles; that is, the ice crystals move as fluid and deform in the first step. Second,
231 the shapes of ice crystals deformed in the first step are restored with keeping the
232 translational and the angular momentums at the centers of gravity points of the crystals.
233 The procedure combining the calculations of incompressible fluid and the ice-water
234 interaction was repeated with time steps, and the interactions between ice crystals (rigid
235 bodies) and fluid were represented.
236
237
238 **2.1.4 Crystal Growth Model**
239
240 Fig. 1 shows a schematic of the crystal growth model introduced into the MPS method.
241 To represent the process where crystal nuclei are generated in supercooled seawater and

grow with a certain growth rate, we employed the following procedure:

(i) We assumed a simulation space that was discretized into m particles.

(ii) All particles are initially given the character number -1, which indicates that they are liquid:

$$\text{character}(i) = -1, \tag{13}$$

where i is the number of a particle.

(iii) Some particles were chosen from the liquid particles and their character number (-1) was changed to k ($k = 1,2,3,\cdots$). The particles with the character number k (≥ 1) were assumed to be solidified. The solidified time t_{s_j}, growth rate $\vec{g}^{(k)}$, crystal orientation $\theta^{(k)}$ and density ρ_s of a solid were defined for the solidified particles.

(iv) The time increment Δt was defined as

$$\Delta t = \frac{\min\left(\left|\vec{r}_j - \vec{r}_i\right|\right)}{\alpha \cdot \max\left(\left|\vec{g}^{(k)}\right|\right)}, \tag{14}$$

where α was the coefficient determining the fineness of time divisions. $\vec{r}$ is the position vector of a particle, and $\left|\vec{r}_j - \vec{r}_i\right|$ is the distance between particles *i* and *j*.

(v) Time durations for solid particles *j* to reach a liquid particle i were calculated and the

shortest time duration $t_{min\,i}$ was found; that is:

$$t_{min\,i} = \min_{j \in J} \left[t_{s\,j} + \frac{\left| \vec{r}_j - \vec{r}_i \right|}{\left| g_{ji}^{(k)} \right|} \right] \quad J = \left\{ j : \left| \vec{r}_j - \vec{r}_i \right| \le r_{cry} \text{ and character}(j) \ne -1 \right\}, \tag{15}$$

where $\left| g_{ji}^{(k)} \right|$ is the growth rate of particle *j* in the direction of particle *i* and r_{cry} is the reachable distance of growth from particles *j* (Fig. 1 (a) and (b)). Character number *k*, which is the character of particle *j*, was also stored.

(vi) If the condition

$$t + \Delta t \ge t_{min\,i} \tag{16}$$

was satisfied, particle i was assumed to be solidified ($\text{character}(i) = k$) at time

$$t_{si} = \begin{cases} t_{min\,i} & \left(if \;\; t \le t_{min\,i} \le t + \Delta t \right) \\ t + \dfrac{\Delta t}{2} & \left(if \;\; t_{min\,i} < t \right) \end{cases}, \tag{17}$$

and $\vec{g}^{(k)}$, $\theta^{(k)}$ and ρ_s were added to particle *i*. An aggregate of particles with the same character number was assumed to be a crystal and treated as a rigid body.

In Eq. (17), the definition of the solidified time $t_{s\,i}$ changes depending on $t_{min\,i}$. The

reason for this is as follows. When $t_{min_i} < t$, if t_{min_i} is employed as t_{s_i}, particle *i* is solidified at the time of the previous step. To avoid conflicts with this problem, we employed a time intermediate between *t* and $t + \Delta t$ if $t_{min_i} < t$. When the above routines were introduced into the MPS method and steps (iv)-(vi) were repeated, crystal nuclei grew (Fig. 1 (c)-(e)) and floated up.

2.1.5 Growth Rate Model of Crystal Nuclei

When the crystal nuclei of ice grow in supercooled seawater, their growth rate in the direction perpendicular to the c-axis is commonly higher than that in the c-axis. Such anisotropy in the growth rates results in discoidal crystals in the initial stage of their growth (e.g., Weeks and Ackley, 1986). To represent the anisotropic growth of nuclei in a two-dimensional approximation, we employed the following model.

Fig. 2 shows the model for the growth rate of the discoidal crystals, when we observed from a direction perpendicular to the c-axis. The growth rates in the direction of and perpendicular to the c-axis can be expressed as

$$\left| \vec{g}_{2d\,basal}^{(k)} \right| = C_1, \tag{18}$$

$$\left|\vec{g}_{2dc}^{(k)}\right| = C_2\,, \tag{19}$$

where C_1 and C_2 are constants. The rotation relation between the global coordinate system $\boldsymbol{x}-\boldsymbol{y}$ and the local coordinate system $\boldsymbol{x_0}-\boldsymbol{y_0}$ of a nucleus *k* is given by $\theta^{(k)}$.

2.2 Voronoi Dynamics Technique

We employ the Voronoi dynamics technique (Ohashi et al., 2004; Kawano and Ohashi, 2009; Dempsey et al., 2010) to simulate crystal growth of sea ice in three-dimensional space. In the technique, crystal growth is that in which each of crystal nuclei extends its territory. The territory is assumed to be a crystal and its extension represents crystal growth. A nucleus will grow faster if it is generated at an earlier nucleation stage and if it is located at a better place for growth; a larger liquid region existing around the nucleus results in a larger crystal.

The Voronoi dynamics technique was developed by Ohashi et al. (2004), and two-dimensional simulations of growth of ice crystals were performed using the method; the crystal fabrics obtained showed good similarity with those of actual ice crystals. The method was adapted to the three-dimensional simulations of crystal growth by Kawano and Ohashi (2009), and development process of sea ice from the sea surface was simulated; the results obtained by the simulations showed that the c-axis orientations as well as crystal

317 fabrics have good similarity with those of actual sea ice. Dempsey et al. (2010)
318 introduced the effect of rotations of crystals after their flotation into the Voronoi dynamics
319 technique; the model successfully predicted the platelet ice fabric in McMurdo Sound,
320 Anterctica. That is, the Voronoi dynamics technique has been adapted mainly to predict
321 the crystal fabrics and c-axis orientations of sea ice. The numerical procedure for the
322 Voronoi dynamics technique is explained below.
323
324 Fig. 3 shows a schematic of the Voronoi dynamics technique, and the algorithm is
325 explained below.
326 (i) We assumed a simulation space $w \times h \times d$ that was divided into $m_x \times m_y \times m_z$.
327 (ii) All cells were initially given the character number -1, which means that the cells were
328 liquid:
329

$$\text{character}(i, j, k) = -1, \tag{20}$$

330
331 where the set of (i, j, k) is the address of a cell.
332 (iii) Nuclei were put into the simulation space. Each had a character number *k*
333 ($k = 1,2,3,\cdots$), nucleation position $\vec{x}_n^{(k)}$, nucleation timing $t_n^{(k)}$ and growth rate
334 $\left|\vec{g}^{(k)}\right|$.
335 (iv) The time increased from *t* to $t + \Delta t$. Δt was calculated by
336

$$\Delta t = \frac{\min(w, h, d)}{\alpha \cdot \max\left(\left|\vec{g}^{(k)}\right|\right)}, \tag{21}$$

where α is the coefficient to determine a fineness of time deviation.

(v) The time $t_{reach}^{(k)}$ when a nucleus has grown from $\vec{x}_n^{(k)}$ to the center $\vec{x}_c(i, j, l)$ of each cell was calculated:

$$t_{reach}^{(k)} = \frac{\left|\vec{x}_c(i, j, l) - \vec{x}_n^{(k)}\right|}{\left|\vec{g}^{(k)}\right|} + t_n^{(k)}. \tag{22}$$

(vi) The number *k* was added to the cell (i, j, l):

$$\text{character}(i, j, l) = k, \tag{23}$$

if following conditions were satisfied:

(a) $t + \Delta t \geq t_{reach}^{(k)}$,

(b) the cell had the character number of liquid (-1), and

(c1) the character number *k* did not exist in all cells or

(c2) at least one of the neighboring cells had the character number *k*.

In the case where some nuclei satisfy the condition (a), the number *k* of the nucleus with smallest value of $t_{reach}^{(k)}$ is selected in those satisfying the condition (c1) or (c2).

353 Cells with a character number *k* were assumed to be solidified. When steps (iv)-(vi)
354 were repeated, aggregates of solidified cells, where each of them has the same
355 character number *k*, were formed. Each aggregate was assumed to be an individual
356 crystal.
357
358 The growth rate model introduced into the Voronoi dynamics technique is as follows; Fig. 4
359 shows a schematic of the model. Crystal nuclei were assumed to grow in discoidal shapes.
360 The growth rates in the direction of and perpendicular to the c-axis can be expressed as
361 follows:
362

$$\left|\vec{g}_{3d\,basal}^{(k)}\right| = C_1, \tag{24}$$

363

$$\left|\vec{g}_{3d\,c}^{(k)}\right| = C_2, \tag{25}$$

364
365 where C_1 and C_2 are constants. The rotation relationship between the global
366 coordinate system $\boldsymbol{x}-\boldsymbol{y}-\boldsymbol{z}$ and the local coordinate system $\boldsymbol{x_0}-\boldsymbol{y_0}-\boldsymbol{z_0}$ of a nucleus *k*
367 was given by a set of Euler angles (κ,θ,ϕ).
368
369
370
371 **3. Results and Discussion**
372

3.1 Flotation and accumulation of crystal nuclei simulated by the MPS method

Let us assume a condition where crystal nuclei are generated in supercooled seawater near the surface of a calm sea. Crystal nuclei float to the sea surface due to buoyancy, grow in a discoidal shape, and accumulate near the sea surface. To represent such conditions, we employed the following conditions.

The two-dimensional seawater specimen employed in this study is shown in Fig. 5 (a). The size of the specimen, which was placed on the wall, is 4×10 mm^2 and discretized by 40 $\times 100$ particles. Next, 100 particles were randomly chosen as crystal nuclei within the upper half of the specimen, and their physical constants were changed from those of seawater to ice. Their growth rate was assumed to be $\left|\vec{g}_{2d\,basal}^{(k)}\right| = 0.1$ mm s^{-1} and $\left|\vec{g}_{2d\,c}^{(k)}\right| = 0.01$ mm s^{-1}, and their initial crystal orientations were randomly selected. The density of ice was given by $\rho_s = 917$ kg m^{-3} and the density of seawater was approximately given by $\rho_l = 1000$ kg m^{-3} which is the value of fresh water. The free slip condition was applied to the boundary between the wall and seawater. A cyclic boundary condition was assumed for both sides of the specimen. The results are shown in Fig. 5 (b)-(d), where different crystal nuclei are shown in different colors.

Crystal nuclei grew with an anisotropic growth rate, and discoidal crystals were formed. At the same time, they moved upward and accumulated near the sea surface. After the

394 accumulation, there was less space to grow around the crystal nuclei, and eventually they
395 stopped their growth. Thus, the obtained crystal fabric shows smaller grains within the
396 upper part of the specimen. The result means that the obtained crystal fabric is formed by
397 the growth, flotation, and accumulation of crystal nuclei.
398
399 Next, we extracted the upper 3.5 mm of the ice crystal in Fig. 5 (d), and the c-axis
400 distribution within the specimen was obtained using the following procedure; the results are
401 shown in Fig. 6. The relative percentages shown in the figure were calculated using the
402 number of crystals. In other words, the c-axes ranging from 0° to 90° were divided into
403 nine bins, and each relative percentage was calculated by the number of crystals belonging
404 to each c-axis section. Fig. 6 shows that a minor peak existed at a nearly vertical ($\theta = 0°$)
405 c-axis, and one more minor peak was observed at around $\theta = 70°$. We noticed that such a
406 distribution was formed by flotation and accumulation of crystal nuclei near the sea surface.
407 In other words, the distribution in Fig. 6 would reflect the mechanism where discoidal
408 crystal nuclei were oriented after their flotation and accumulation. However, the
409 differences between the bins in Fig. 6 were modest, and there is a possibility that the
410 distribution is changed depending on the simulation conditions such as nucleation density,
411 growth rate, and growth rate anisotropy.
412
413
414 **3.2 Development process of sea ice crystals simulated by the Voronoi dynamics**
415 **technique**

Using the Voronoi dynamics technique, we numerically simulated the development process of sea ice crystals from the accumulated layer of crystal nuclei near the sea surface. The simulation conditions were as follows. The size of the seawater specimen was $100 \times 100 \times 100$ mm^3 and discretized by $100 \times 100 \times 100$ voxels. Nine hundred nuclei were placed within the upper 10 mm of the sea surface. Two simulations were performed with different c-axis orientations of initial crystal nuclei; one was given by the c-axis distribution obtained by the simulation of flotation and accumulation of crystal nuclei (Fig. 6) and the other was randomly selected. Growth rate parameters employed in both simulations were assumed to be $\left|\vec{g}_{3d\,basal}^{(k)}\right| = 0.1 \ \ \mathrm{mm\,s^{-1}}$ and $\left|\vec{g}_{3d\,c}^{(k)}\right| = 0.01 \ \ \mathrm{mm\,s^{-1}}$.

Fig. 7 shows the development process of sea ice fabrics: (a)-(c) are the results obtained with the condition where c-axis orientations of initial nuclei were given by Fig.6 and (d)-(f) are the results obtained with the condition where c-axis orientations of initial nuclei were randomly given. In other words, the effects of flotation of the initial nuclei were considered in the simulations of Fig. 7 (a)-(c). The effects of flotation were investigated by comparing the results of the two simulations.

Both results show fine grains near the sea surface and columnar grains below it, and their appearances have good similarity with each other. Fig. 8 shows changes in the c-axis distributions with depth; the distributions were calculated with areas of crystals and their c-axes within each horizontal cross-section. In both conditions with and without

438 considering the effect of flotation of crystal nuclei, only c-axes close to the horizontal
439 remain at greater depths, i.e., geometric selection of c-axis orientations takes place. This
440 transition process is in good agreement with that of actual sea ice (see Fig. 9). Kawano
441 and Ohashi (2009) and Dempsey et al. (2010) also successfully reproduced the
442 phenomenon using the Voronoi dynamics technique. In the c-axis distributions near the
443 sea surfaces, however, there was a little difference between the results obtained with and
444 without considering the effects of flotation and accumulation of crystal nuclei.
445
446 Fig.8 (a) and (d) shows c-axis distributions within the horizontal plane 5 mm from the top
447 of the ice. The result obtained with the condition where initial crystal nuclei were
448 randomly selected is a relatively homogeneous distribution (Fig. 8 (d)), whereas there are
449 two minor peaks at the vertical c-axis and 70° in the result obtained by the simulation
450 considering the effect of flotation (Fig. 8 (a)). The features of Fig. 8 (a) are also observed
451 in that of an actual sea ice (Fig. 9 (a)), and we notice that the c-axis distribution is
452 successfully reproduced by the simulation considering flotation of crystal nuclei.
453
454
455 **3.3 Effects of flotation and geometric selection on c-axis distribution**
456
457 From the above discussion, it was indicated that flotation and accumulation of crystal
458 nuclei strongly affect the c-axis distributions of sea ice near the sea surface. However,
459 one point still unclear; crystal nuclei with a nearly vertical c-axis should grow faster and

460 occupy a larger area than those with c-axes in horizontal plane within the horizontal
461 cross-sections; however, the c-axis distribution calculated by the number of initial nuclei
462 (Fig. 6) was similar to that calculated by the area of crystals (Fig. 8 (a)). Next, we
463 investigated the reason for such a similarity.
464
465 Fig. 10 (a) and (b) shows relative percentages of the average areas and the number of
466 crystals within the horizontal cross-section 5 mm from the top of the ice studied in Fig. 7
467 (c); each relative percentage in the histograms was calculated using crystals belonging to
468 each c-axis section. Fig. 10 (a) shows that crystals with vertical and nearly vertical c-axes
469 occupy a larger area than others. In contrast, Fig. 10 (b) shows a peak at around 70° and
470 the number of crystals with a nearly vertical c-axis is lower than that of others. Thus,
471 while the number of crystals with vertical c-axis is lower than that of others within the
472 horizontal cross-section near the sea surface, crystals with the vertical c-axis have a faster
473 growth rate and occupy a larger area within the horizontal cross-section. In the case of the
474 crystals with c-axis around 70°, the number was higher, but the area of each crystal was
475 smaller due to its slower growth rate in the horizontal direction. In other words, the
476 geometric selection of c-axes occurs also within the layer of fine-grained ice near the sea
477 surface. As a result, the c-axis distribution of Fig. 8 (a) was obtained.
478
479 Fig. 11 shows a schematic of the changes in areas and the appearance ratio of crystals
480 depending on their c-axis orientations in the horizontal cross-sections. Within the
481 horizontal cross-sections, c-axis vertical crystals occupy larger area, while their appearance

ratio is lower; the same phenomenon can be observed in the actual sea ice (e.g. Dempsey and Langhorne, 2012). We noticed that crystal orientations of crystal nuclei were determined by the effect of flotation and accumulation, and the areas and number of crystals within the horizontal cross-sections were geometrically determined by their orientations (Fig. 11). Therefore, the results indicate that both the effects of flotation and accumulation of the crystal nuclei and geometric selection of c-axes are dominant factors in determining the c-axis distributions within the horizontal cross-sections of the surface layer of ice grown under calm sea conditions, which results in the c-axis distribution observed by Weeks and Ackley (1986).

4. Conclusions

We conducted numerical simulations of the development process of sea ice from the sea surface in a calm sea considering flotation and accumulation of crystal nuclei using the Moving Particle Semi-implicit (MPS) method and the Voronoi dynamics technique. The results can be summarized as follows.

With the MPS method, we successfully reproduced a process where discoidal crystal nuclei grew with their flotation and accumulation near the sea surface. The c-axis distribution in

503 the accumulated layer of crystal nuclei calculated by the number of crystal nuclei showed
504 two minor peaks: one was at the horizontal c-axis and the other was at around 70°.
505
506 The c-axis distribution obtained by the MPS method adapted to initial crystal nuclei, and
507 sea ice crystal growth from the sea surface was simulated by the Voronoi dynamics
508 technique. The results showed good agreement with an experimental result; two minor
509 peaks occurred in the c-axis distribution within the horizontal cross-section of the sea ice
510 near the sea surface. In contrast, some discrepancy occurred in the distribution with the
511 condition where c-axes of initial crystal nuclei were randomly selected. Thus, more
512 accurate c-axis distribution near the sea surface was reproduced by using a model
513 combining the Voronoi dynamics technique and the effect of flotation and accumulation of
514 crystal nuclei
515
516 The c-axis distribution calculated by the number of crystal nuclei after their flotation and
517 accumulation was similar to that calculated by the area of crystals within the horizontal
518 cross-section near the sea surface. However, the process of flotation and accumulation of
519 crystal nuclei did not directly determine the c-axis distribution within the horizontal
520 cross-section; the number of crystals with the vertical c-axis and nearly vertical c-axes was
521 lower within the section, but their average area within the horizontal cross-sections was
522 larger than that of other grains. In other words, the results obtained indicated that the
523 effects of flotation and accumulation as well as the geometric selection of c-axes by a
524 favorable crystal orientation were the dominant factors in determining the c-axis

distribution of a surface layer of ice grown under calm sea conditions: this resulted in the c-axis distribution observed by Weeks and Ackley (1986).

In this study, we successfully reproduced the development process of sea ice crystals from the surface of calm sea with considering the effects of flotation and accumulation of initial crystal nuclei, using a model combining the MPS method and Voronoi dynamics. The model could deal with the ice-water mixture such as frazil and grease ice; it would be adapted to investigate their solid fractions that are fiendishly difficult to measure, by introducing some physical effects into it. There is a possibility that the improved model is also adapted to analyze the fresh water ice; it would be useful for investigating preferred crystal orientation (e.g. Müeller-Stoffels et al., 2009). This work would be an important step for the development of numerical models to predict the complex phenomena of sea ice depending on the microstructure, such as behavior of the ice-water mixture on the sea surface.

Acknowledgements

We would like to express my gratitude to Toshiyuki Kawamura and Masafumi Sasaki for insightful discussions. Meaningful comments from two anonymous reviewers improved the quality of the manuscript. This work was financially supported by the National

Institute of Technology, Asahikawa College, Hokkaido, Japan, and by the Calculation Mechanics Laboratory, Kitami Institute of Technology, Hokkaido, Japan.

References

Ataie-Ashtiani, B., Farhadi, L., 2006. A stable moving-particle semi-implicit method for free surface flows. Fluid Dynamics Research 38, 241-256.

Cole, D.M., 2001. The microstructure of ice and its influence on mechanical properties. Engineering Fracture Mechanics 68, 1797-1822.

Dempsey, D.E., Langhorne, P.J., Robinson, N.J., Williams, M.J.M., Haskell, T.G., Few, R.D., 2010. Observation and modeling of platelet ice fabric in McMurdo Sound, Antarctica. Journal of Geophysical Research 115 (C1), 1-16.

Dempsey, D.E., Langhorne, P.J., 2012. Geometric properties of platelet ice crystals. Cold Regions Science and Technology 78, 1-13.

Eicken, H., 2003. Growth, microstructure and properties of sea ice. In: Thomas, D.N. and Dieckmann, G.S. (Eds.), Sea ice: An introduction to its physics, chemistry, biology and geology. Blackwell, Oxford, 22–81.

Golden, K.M., Ackley, S.F., Lytle, V.I., 1998. The percolation phase transition in sea ice. Science 282, 2238-2241.

568 Gotoh, H., Sakai, T., 2006. Key issues in the particle method for computation of wave
569 breaking. Coastal Engineering 53, 171-179.
570 Gow, A. J., Tucker III, W.B., 1991. Physical and dynamic properties of sea ice in the polar
571 oceans. Monograph 91-1, U.S. Army Cold Regions Research & Engineering Laboratory.
572 Jones, K.A., Ingham, M., Eicken, H., 2012. Modeling the anisotropic brine microstructure
573 in first-year Arctic sea ice. Journal of Geophysical Research 117 (C2), 1-14.
574 Kawano, Y., Ohashi, T., 2009. A mesoscopic numerical study of sea ice crystal growth and
575 texture development. Cold Regions Science and Technology 57 (1), 39-48.
576 Kawano, Y., Ohashi, T., 2013. Two-dimensional numerical study on the growth of sea ice
577 crystals with flotation of crystal nuclei and its c-axes distribution. Proceedings of the 8th
578 Pacific Rim International Congress on Advanced Materials and Processing, Waikoloa,
579 Hawaii, USA, 2839-2846.
580 Kondo, M., Koshizuka, S., 2007. Suppressing pressure oscillation in MPS. Proceedings of
581 the 20th Computational Mechanics Conference, 463-464. (in Japanese).
582 Koshizuka S., Ikeda H. and Oka Y., Numerical analysis of fragmentation mechanisms in
583 vapor explosions, Nucl. Eng. Des. **189**, 1999, 423-433.
584 Koshizuka, S., Nobe, A., Oka, Y., 1998. Numerical analysis of breaking waves using the
585 moving particle semi-implicit method. International Journal for Numerical Methods in
586 Fluids 26, 751-769.
587 Koshizuka, S., Oka, Y., 1995. Moving particle semi-implicit method: a gridless approach
588 based on particle interactions for incompressible flow simulation. Proceedings of the 3rd
589 Workshop on Supersimulators for Nuclear Power Plants, Tokyo, Japan, 43-49.

590 Koshizuka, S., Oka, Y., 1996. Moving-particle semi-implicit method for fragmentation of
591 incompressible fluid. Nuclear Science and Engineering 123, 421-434.
592 Lee, C.J.K., Noguchi, H., Koshizuka S., 2007. Fluid-shell structure interaction analysis by
593 coupled particle and finite element method. Computers and Structures 85, 688-697.
594 Martin, S., 1981. Frazil ice in rivers and oceans. Annual Review of Fluid Mechanics 13,
595 379-397.
596 Maus, S., De la Rosa, S., 2012. Salinity and solid fraction of frazil and grease ice. Journal
597 of Glaciology 58 (209), 594-612.
598 Müller-Stoffels, M., Langhorne, P.J., Petrich, C., Kempema, E.W., 2009. Preferred crystal
599 orientation in fresh water ice. Cold Regions Science and Technology 56, 1-9.
600 Naumann, A.K., Notz, D., Håvik, L., Sirevaag, A., 2012. Laboratory study of initial sea-ice
601 growth: properties of grease ice and nilas. The Cryosphere 6, 729-741.
602 Ohashi, T., Sasaki, M., Yoshimura, Y., 2004. A numerical simulation of the development
603 of ice-microstructure. Proceedings of the 19th International Symposium on Okhotsk Sea
604 & Sea Ice, 180-185.
605 Petrich, C, Langhorne, P.J., Sun, Z.F., 2006. Modeling the interrelationships between
606 permeability, effective porosity and total porosity in sea ice. Cold Regions Science and
607 Technology 44, 131-144.
608 Schulson, E.M., 1999. The structure and mechanical behavior of Ice. The Journal of the
609 Minerals, Metals and Materials Society 51 (2), 21-27.
610 Shao S., Lo, E.Y.M., 2003. Incompressible SPH method for simulating Newtonian and
611 non-Newtonian flows with a free surface. Advances in Water Resources 26, 787-800.

612 Skogseth, R., Nilsen, F., Smedsrud, L.H., 2009. Supercooled water in an Arctic polynya:
613 observations and modeling. Journal of Glaciology 55 (189), 43-51.
614 Smedsrud, L.H., Skogseth, R., 2006. Field measurements of Arctic grease ice properties
615 and processes. Cold Regions Science and Technology 44, 171-183.
616 Ushio, S., Wakatsuchi M., 1993. A laboratory study on supercooling and frazil ice
617 production processes in winter coastal polynyas, Journal of Geophysical Reserch 98
618 (C11), 20321-20328.
619 Weeks, W.F., 1998. Growth conditions and the structure and properties of sea ice. In:
620 Leppäranta, M. (Ed.), Physics of Ice-covered Seas, Helsinki University Press, Helsinki,
621 25-104.
622 Weeks, W.F., Ackley, S.F., 1986. The growth, structure and properties of sea ice. In:
623 Untersteiner, N., (Ed.), The Geophysics of Sea Ice, Plenum Press, New York, 9-164.
624 Weeks, W.F., Wettlaufer, J.S., 1996. Crystal orientations in floating ice sheets. The
625 Johannes Weertman's Symposium, R.J. Arsenault *et al. (Eds.)*, The Minerals, Metals &
626 Materials Society, 337–350.
627 Zhang, Y., Wilson, C.J.L., 1997. Lattice rotation in polycrystalline aggregates and single
628 crystals with one slip system: a numerical and experimental approach. Journal of
629 Structural Geology 19 (6), 875-885.
630
631
632
633 **Figure Captions**

Figure 1. Schematic of the crystal growth model introduced into the moving particle semi-implicit method; (a), (b) the growth process of single crystal and (c)-(e) a tri-crystal. An aggregate with the same character number is an individual crystal.

Figure 2. Anisotropic growth rate model and local coordinate system $x_0 - y_0$ defined for each of the crystal nuclei. The model was introduced into the moving particle semi-implicit method.

Figure 3. Schematic of the Voronoi dynamics technique (Kawano and Ohashi, 2009).

Figure 4. Growth rate model of a crystal nucleus and its local coordinate system $x_0 - y_0 - z_0$ defined for each crystal nucleus (Kawano and Ohashi, 2009). The model was introduced into the Voronoi dynamics technique.

Figure 5. Flotation and accumulation processes of crystal nuclei simulated using the moving particle semi-implicit method: (a) initial state and (b)-(d) development processes.

Figure 6. Histogram showing the relative percentages of the number of crystals belonging to different c-axis orientations (0° =vertical, 90° =horizontal) in the ice studied in Fig. 5 (d).

Figure 7. Development process of sea ice fabrics obtained by simulations (a)-(c) considering and (d)-(f) without considering the effects of flotation of crystal nuclei.

Figure 8. Histograms showing the relative percentages of different c-axis orientations (0° =vertical, 90° =horizontal) calculated from the area within horizontal cross-sections. Results obtained by simulations (a)-(c) with and (d)-(f) without considering the effects of flotation.

Figure 9. Histograms showing the relative percentages of different c-axis orientations (0° = vertical, 90° = horizontal), which is an experimental observation of actual sea ice grown under calm sea conditions (Weeks and Ackley, 1986).

Figure 10. Histograms showing the relative percentages of (a) average areas of crystals and (b) the number of crystals depending on c-axis orientations (0°= vertical, 90°= horizontal) within the horizontal cross-section 5 mm from the top of the ice studied in Fig.7 (c). The largest value in the relative percentages of each histogram is displayed as 100 %.

Figure 11. Schematic showing the changes of appearance ratio and areas of crystals depending on their c-axis orientations at horizontal cross-sections.

Figures

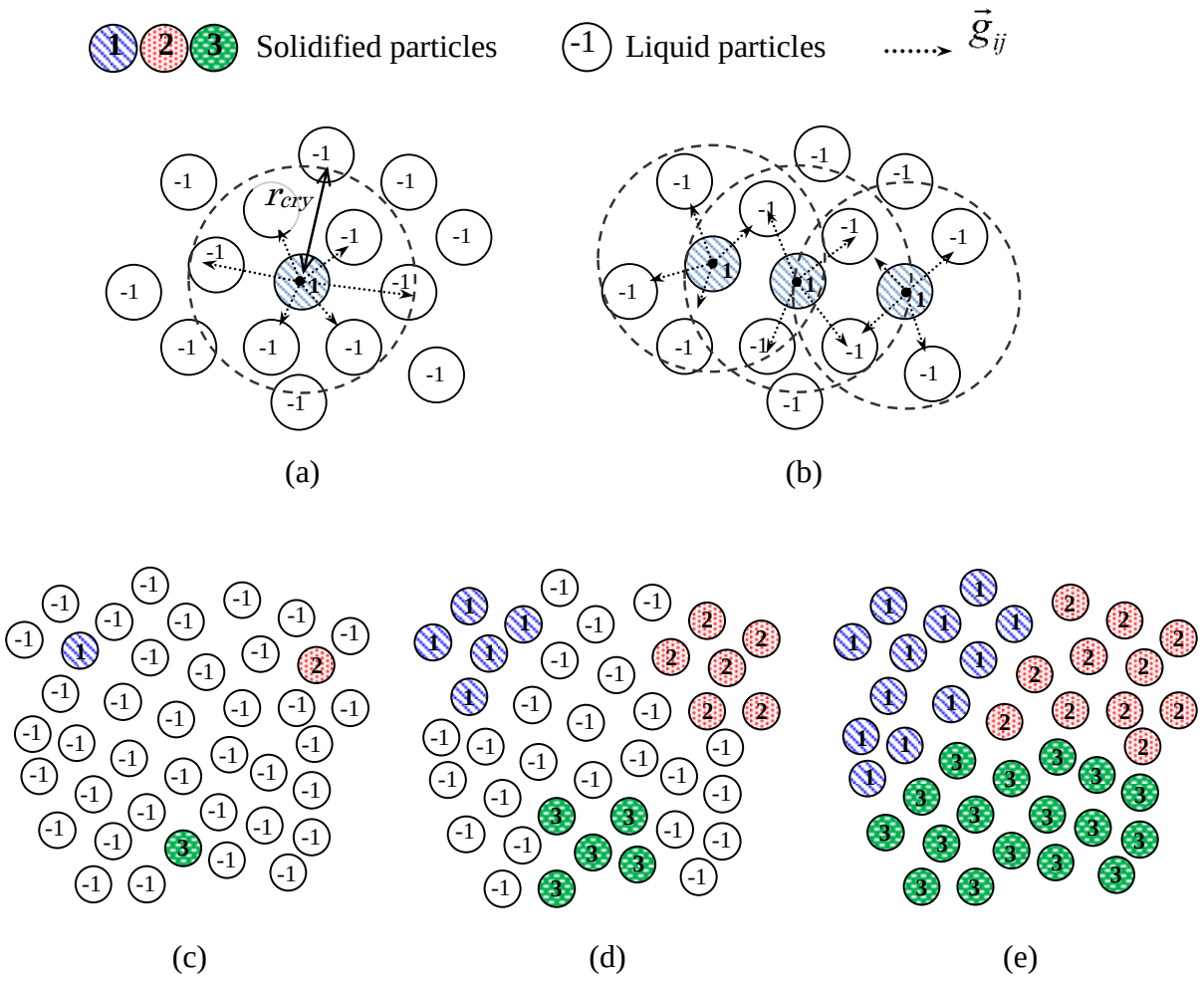

Figure 1. Schematic of the crystal growth model introduced into the moving particle semi-implicit method; (a), (b) the growth process of single crystal and (c)-(e) a tri-crystal. An aggregate with the same character number is an individual crystal.

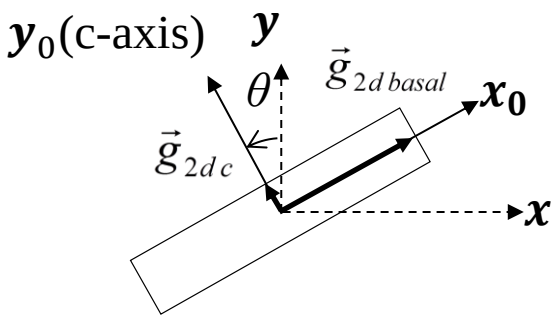

Figure 2. Anisotropic growth rate model and local coordinate system x_0-y_0 defined for each of the crystal nuclei. The model was introduced into the moving particle semi-implicit method.

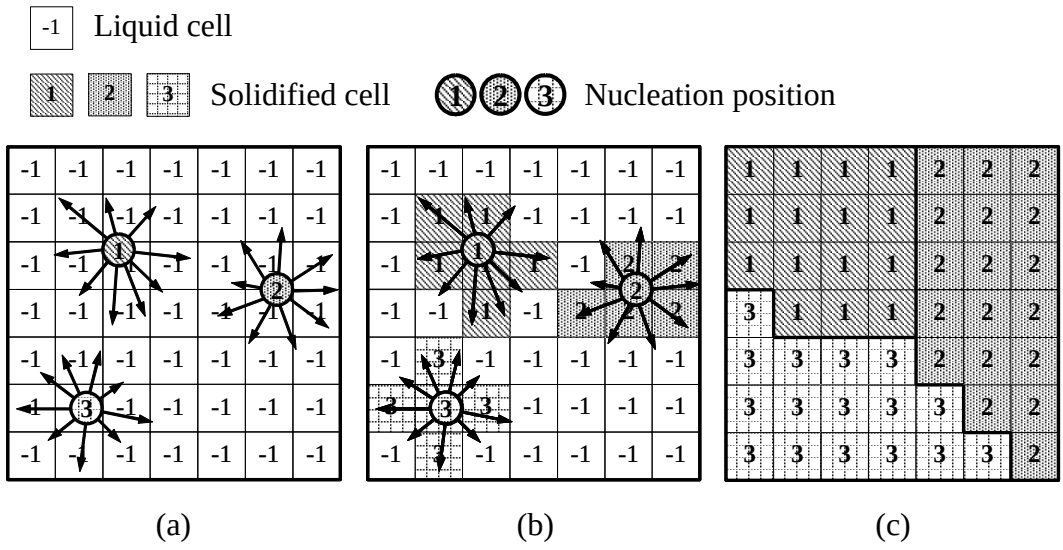

Figure 3. Schematic of the Voronoi dynamics technique (Kawano and Ohashi, 2009).

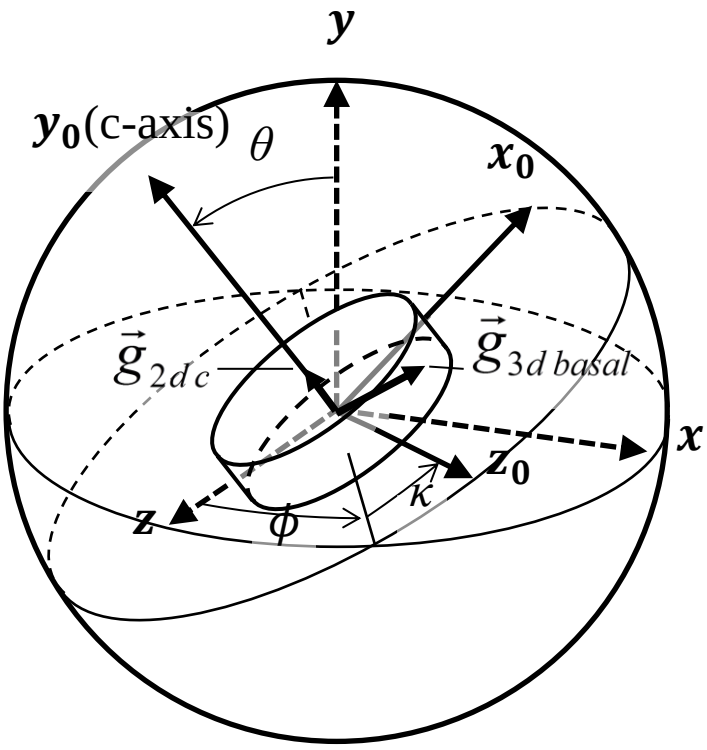

744

745

746 Figure 4. Growth rate model of a crystal nucleus and its local coordinate system

747 $x_0 - y_0 - z_0$ defined for each crystal nucleus. The model was introduced into the Voronoi

748 dynamics technique.

749

750

751

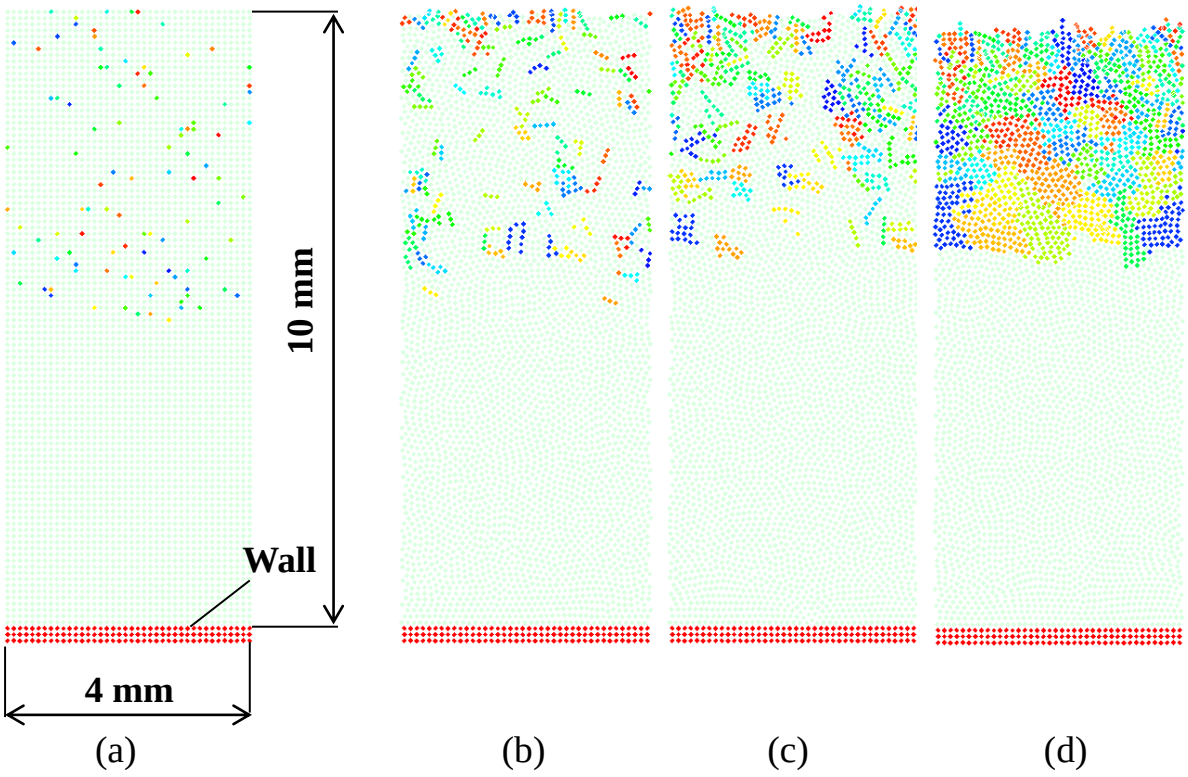

Figure 5. Flotation and accumulation processes of crystal nuclei simulated using the moving particle semi-implicit method: (a) initial state and (b)-(d) development processes.

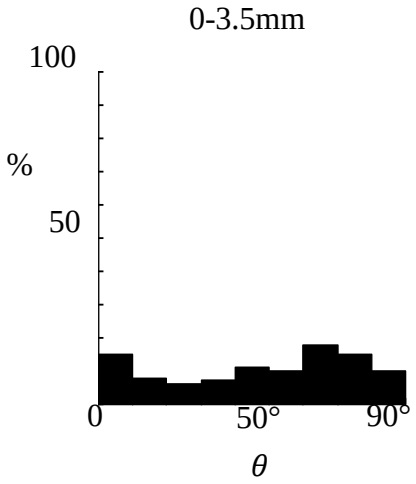

Figure 6. Histogram showing the relative percentages of the number of crystals belonging to different c-axis orientations (0° =vertical, 90° =horizontal) in the ice studied in Fig. 5 (d).

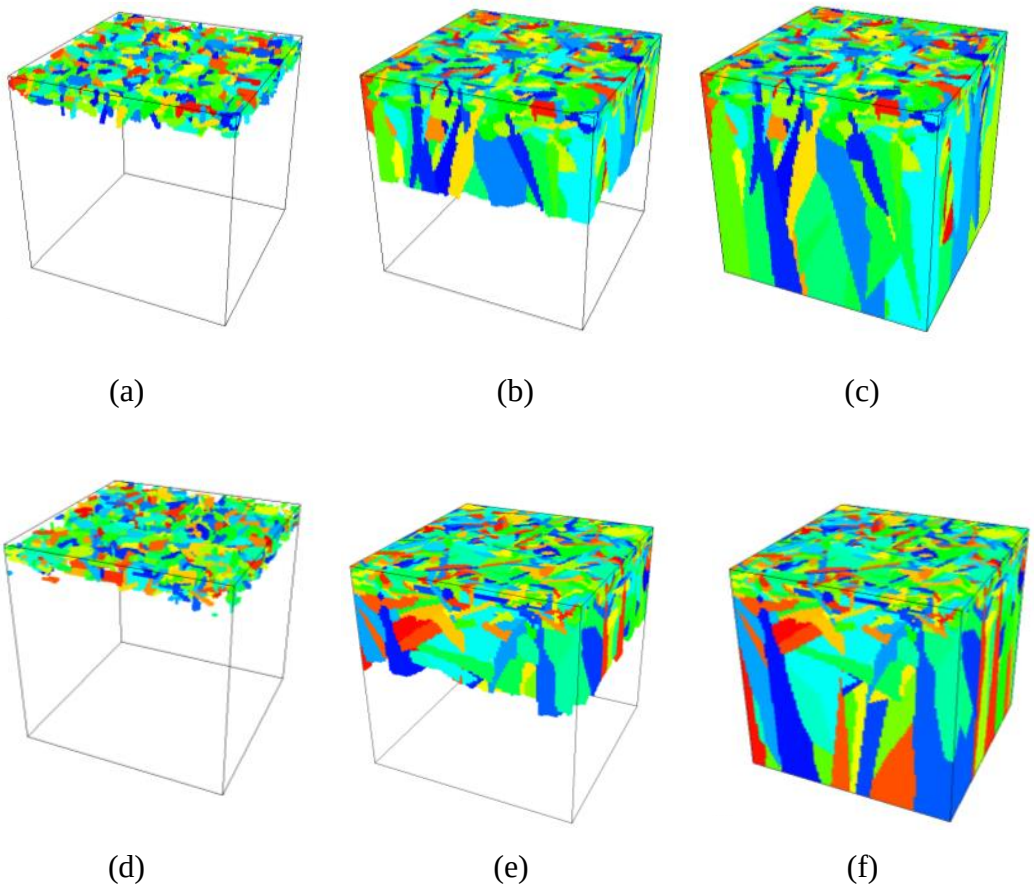

Figure 7. Development process of sea ice fabrics obtained by simulations (a)-(c) considering and (d)-(f) without considering the effects of flotation of crystal nuclei.

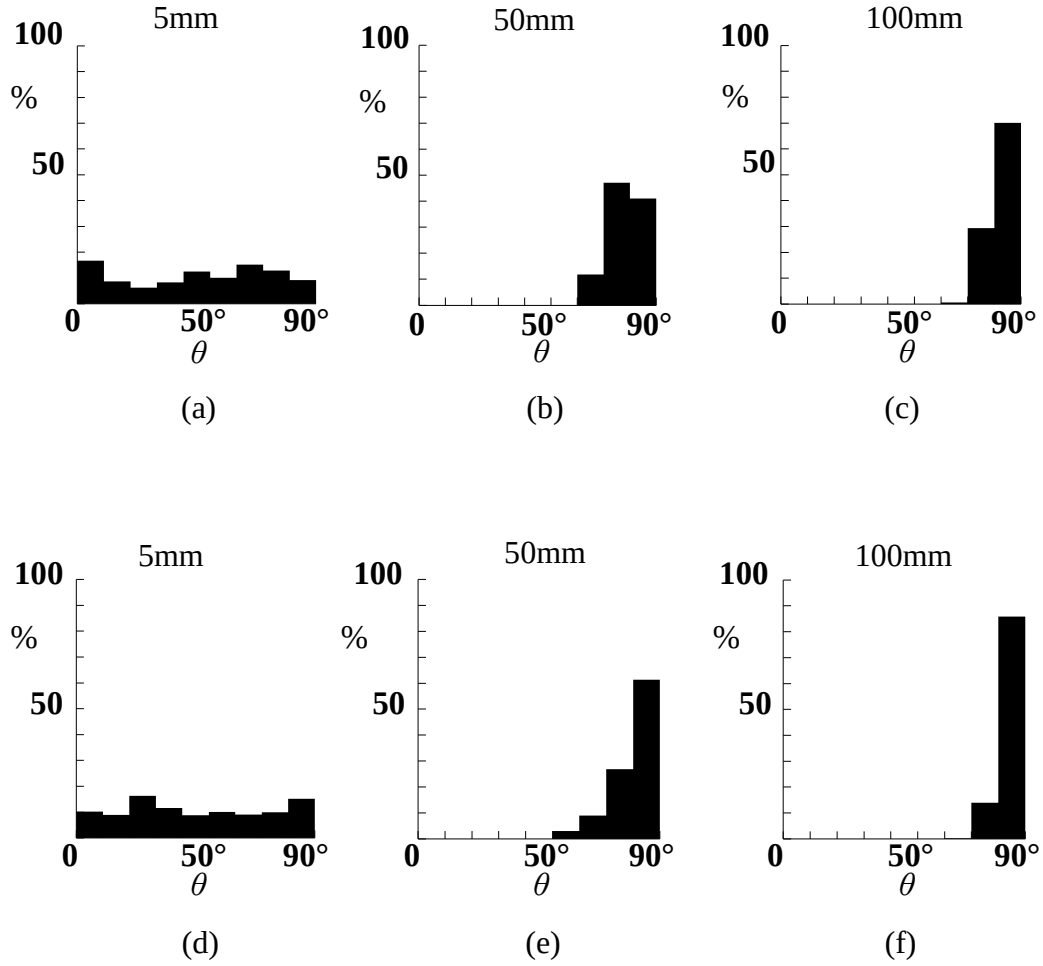

Figure 8. Histograms showing the relative percentages of different c-axis orientations (0° =vertical, 90° =horizontal) calculated from the area within horizontal cross-sections. Results obtained by simulations (a)-(c) with and (d)-(f) without considering the effects of flotation.

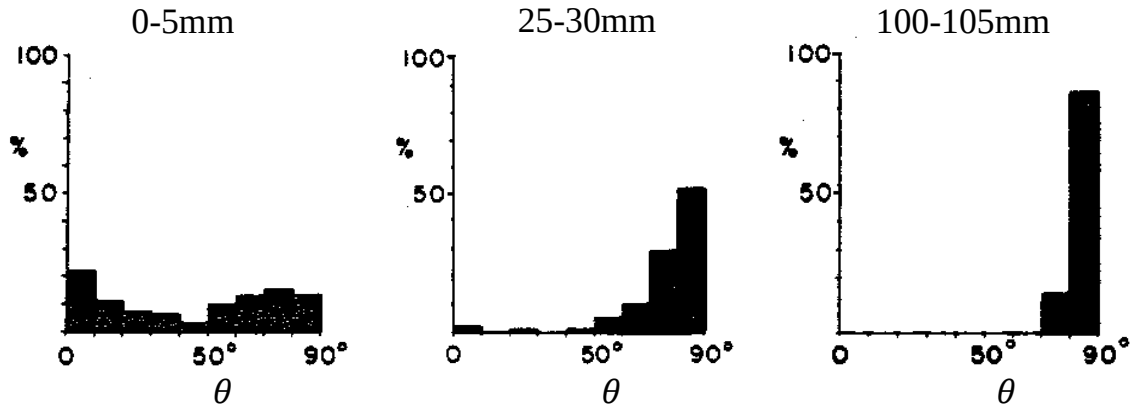

Figure 9. Histograms showing the relative percentages of different c-axis orientations (0° = vertical, 90° = horizontal), which is an experimental observation of actual sea ice grown under calm sea conditions (Weeks and Ackley, 1986).

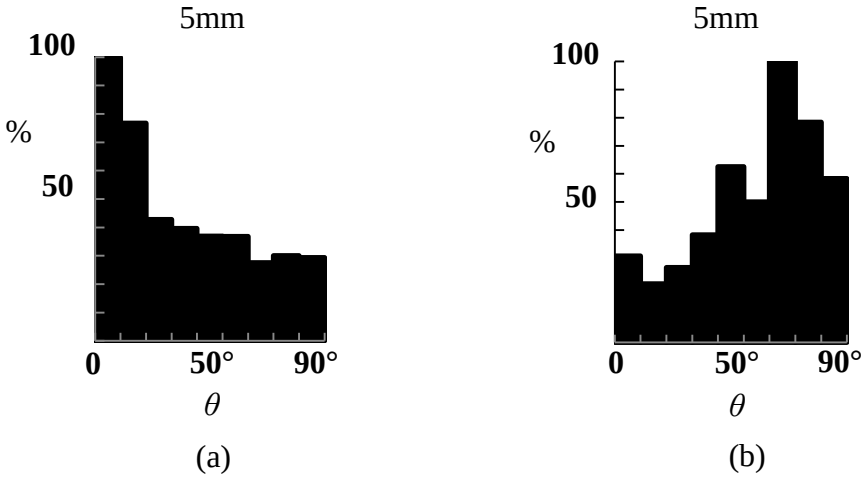

Figure 10. Histograms showing the relative percentages of (a) average areas of crystals and (b) the number of crystals depending on c-axis orientations (0° = vertical, 90° = horizontal) within the horizontal cross-section 5 mm from the top of the ice studied in Fig.7 (c). The largest value in the relative percentages of each histogram was displayed as 100 %.

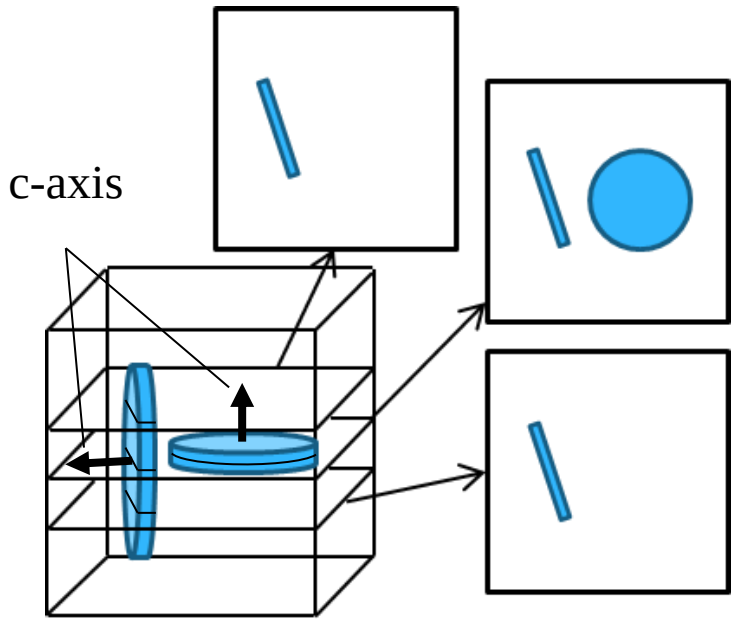

Figure 11. Schematic showing the changes of appearance ratio and areas of crystals depending on their c-axis orientations at horizontal cross-sections.